Title: Application of zinc oxide nanomaterials to improve efficiency of fuel consumption

Authors: Edy Suryono, Ignatius Henry Adi Nagoro, Albanus Bagus Prasojo Nefo

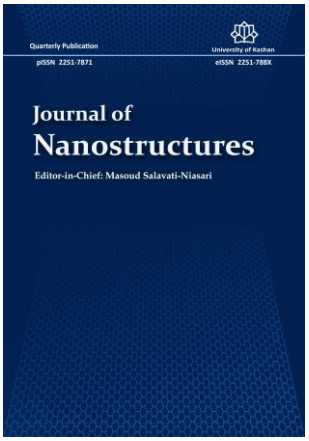


Reference: JNS-2203-2525

To appear in: *Journal of Nanostructures*

**Application of zinc oxide nanomaterials to improve efficiency of fuel consumption**

Edy Suryono*, Ignatius Henry Adi Nagoro, Albanus Bagus Prasojo Nefo

Mechanical Engineering Department, Sekolah Tinggi Teknologi Warga Surakarta, Indonesia

*Corresponding authors email address: edysuryono@sttw.ac.id

**Abstract**

Technology based on ZnO nanomaterials in vehicle fuel systems called Nano Fuel System that reduces fuel consumption and minimize exhaust emissions was studied in the present work. The fuel before entering the fuel chamber was conditioned at certain temperature and pressurized. So that the fuel can be fogged up to reach nano size. The research was expected to produce engine performance with reduced exhaust emissions and more fuel economy. The model was a heated fuel tank that serves to convert liquid fuel into a gas phase. It was conducted by heating fuel at temperatures of 25, 50, 75, and 100 $^{o}$C as well as in pressure conditions of 1, 3, 5, and 7 bar. Initial preparation of the test equipment includes injector test bench and tune-up the engine, while test equipment in the form of emissions test and acceleration test was carried out as a parameter to determine the success rate of the experiment. CO levels decreased as the average fuel temperature rose by 7% at 3 bar pressure and 25.45 % at 5 bar pressures. This indicates that the presence of a heated fuel tank will increase combustion process so that fuel consumption will be more efficient. The levels of carbon dioxide emissions produced indicate that they are below the standard limits of $CO_2$ emissions. The well-installed heated fuel tank worked well as it was seen at the lowest HC level drop at 100 $^{0}$C with a 3000rpm spin of 6.23 %. This indicates fuel consumption is increasingly efficient.

**Keywords:** ZnO, Nano fuel system, heating tank, Fuel consumption.



## 1. Introduction

Increased fuel consumption of vehicles is one of the consumer factors in choosing a vehicle. Many manufacturers innovate in creating automotive products that can reduce fuel consumption as low as possible, and an environmentally clean fuel suitable for use in power engineering [1-3]. The purpose of vehicle innovation, in general, is to improve the performance of the vehicle in terms of optimal fuel use, power produced, and exhaust pollutants [4-5]. The Hydrocarbon Crack System (HCS) is a heat transmission system that uses a catalyst to break the atomic link between carbon (C) and hydrogen ($H_2$). Hydrocracking is a method to improve combustion efficiency[6], thus reducing fuel consumption. Experiments with breaking down carbon bonds in hydrocarbons

(HC) to improve the breakdown of Hydrogen atoms, thereby accelerating the combustion process. The HCS study used copper pipes, a length resulting in the most optimal reduction in fuel consumption and lowering CO emissions, and vehicle power can be increased [7]. Fuel treatment using HCS can produce hydrogen gas ($H_2$) with high concentrations [8]. David [9] has also made HCS in the form of a fixed bed reactor with the principle of converting biogas into new high hydrogen gas. Preheating the fuel [10-12] is one of the efforts to improve engine performance [13]. The perfection of the combustion process depends heavily on the temperature of the fuel mixture. Preheat treatment was used in the HCS method to minimize fuel consumption and enhance engine efficiency. This is influenced by the increased concentration of hydrogen gas in the fuel as long as it was heated [14]. This research was used HCS reactors as Nano Fuel System (NFS) technology installed after the vehicle's main fuel tank. The experiment was conducted by creating a heated fuel tank, with variable temperatures and pressures.

## 2. Materials and methods

Tank testing was carried out for leaks by providing water, whether there is seepage or not. The main components of the tank consist of; heating unit, thermoreader, fuel tank, gas tank, heat sink unit, tank cover, and wiring circuit. Fuel heating was carried out in the heating section with variations of 25, 50, 75, and 100 ºC and under pressure conditions of 1, 3, 5, and 7 bar. The reality in the field at a pressure condition of 1 bar the engine can only operate in stationary conditions, whereas if the gas is opened the engine will stop operating. Meanwhile, at 7 bar, the fuel supply hose will burst. So that this research is obtained at a pressure of 3 and 5 bar. The result of heating in the form of fuel vapor will be accommodated in the gas tank section which is then channeled to the engine combustion section using an injector. Testing exhaust emissions and fuel consumption using a gas analyzer.

### 2.1. Synthesis of ZnO nanoparticles

For the preparation of ZnO nanoparticles, 1 g of $Zn(NO_3)_2.6H_2O$ (MW=297.48 $gmole^{-1}$) was ground in a mortar and then transferred into a 25 mL crucible. Then the sample was treated thermally at 500 ºC for 6 h in a preheated furnace. The final product was cooled normally in the furnace to the room temperature.

## 3. Results and discussions

Figure 1a exhibits the FTIR spectrum of ZnO nanoparticles that indicated two prominent and lower intense peaks along the region from 4,000 to 400 $cm^{-1}$. The corresponding broad peak at 3,460 $cm^{-1}$ was recognized as the stretching vibration of the surface O–H bonds of ZnO nanoparticles. A sharp peak observed at 490 $cm^{-1}$, which

can be credited to overlapping the stretching vibrations of Zn–O bonds corresponding to the tetrahedral and octahedral structures of the ZnO nanoparticles. The FTIR from 430 to 420 $cm^{-1}$ assigned to the Zn–O stretching vibration of the tetrahedral structure of the ZnO nanoparticles while the Zn–O stretching vibration of their octahedral structure lies between 540 and 620 $cm^{-1}$. As observed peak assigned to Zn–O stretching vibrations was in good agreement to the previous studies32, 33. It was confirmed that in both cases of ZnO nanorods, this extreme Zn–O stretching vibration (490 $cm^{-1}$) rests between 507 and 423 $cm^{-1}$. At the same time, the spherical ZnO NPs illustrated a maximum overlapping at 471 $cm^{-1}$ [15-17]. Furthermore, the FTIR spectrum of ZnO nanoparticle exhibits two lower intense peaks at 1627 and 1,377 $cm^{-1}$ owing to organic contaminations arising from intermediates of a reaction, which is considered as a complex of zinc-hydroxo acetates [18-20] or cluster of tetranuclear oxo Zn acetate ($Zn_4O(CH3COO)_6$). The XRD pattern of synthesized ZnO nanoparticles is illustrated in Fig. 1b, showed distinctive diffraction peaks of ZnO NPs for 2θ values of 31.6, 34.3, 36.8, 48.1, 57.4, 63.2, 66.8, 68.1, 69.3, 73.4, and 77.6 with respect to the corresponding crystallographic planes (100), (002), (101), (102), (110), (103), (200), (112), (201), (202) and (104). Scherrer equation was used to determine the crystallite size recorded to be around 22.5 nm. The XRD pattern of the ZnO nanoparticle exhibited enhancement of the diffraction maxima at 2θ value of 34.3 along with the crystallographic plane (002) direction compared to other directions excluding (100) and (101) (c-axis) [21]. The preferential growth of wurtzite rods was observed through the intensity of the crystallographic plane, and this observation was in agreement with the previous studies40.

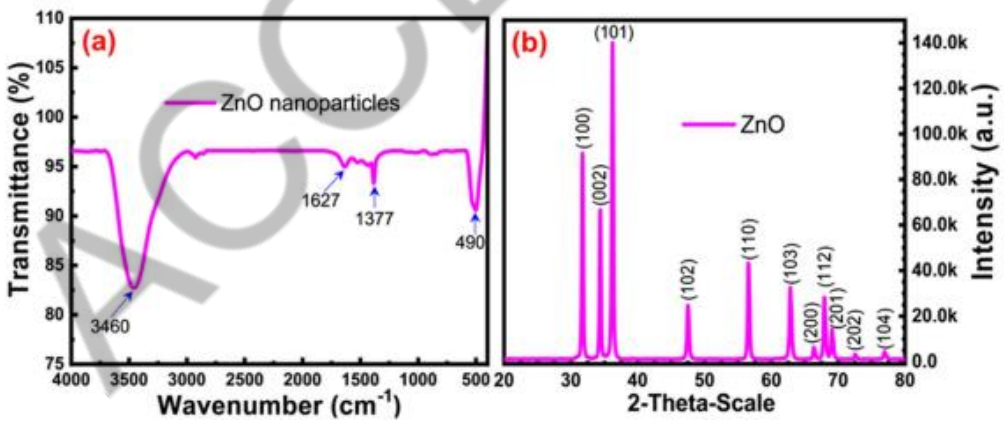


Figure 1. Structural characterization of zinc oxide nanoparticle (a) Fourier transform infrared spectroscopy (FTIR) analysis, (b) X-ray diffraction (XRD) pattern.

The EDX analysis illustrated in Figure 2 c was carried out using Nova Nano FEG-SEM 450; it was identified that three peaks were representing the existence of the Zn with the sharp and intense peaks at 1.0 keV and weak intense peaks at 0.1 keV, respectively. The oxygen element, a counterpart of Zn atom of ZnO nanoparticle exhibited a

peak at 0.5 keV. Besides, a negligible amount of Al and C were observed at corresponding peaks 1.5 keV and 0.8 keV, respectively. These results suggest that the prepared sample contains strong zinc and oxygen signals with a feeble signal of impurities, which may be presented through the precursors. Consequently, it was confirmed the tested sample had high purity of the synthesized ZnO nanoparticles.

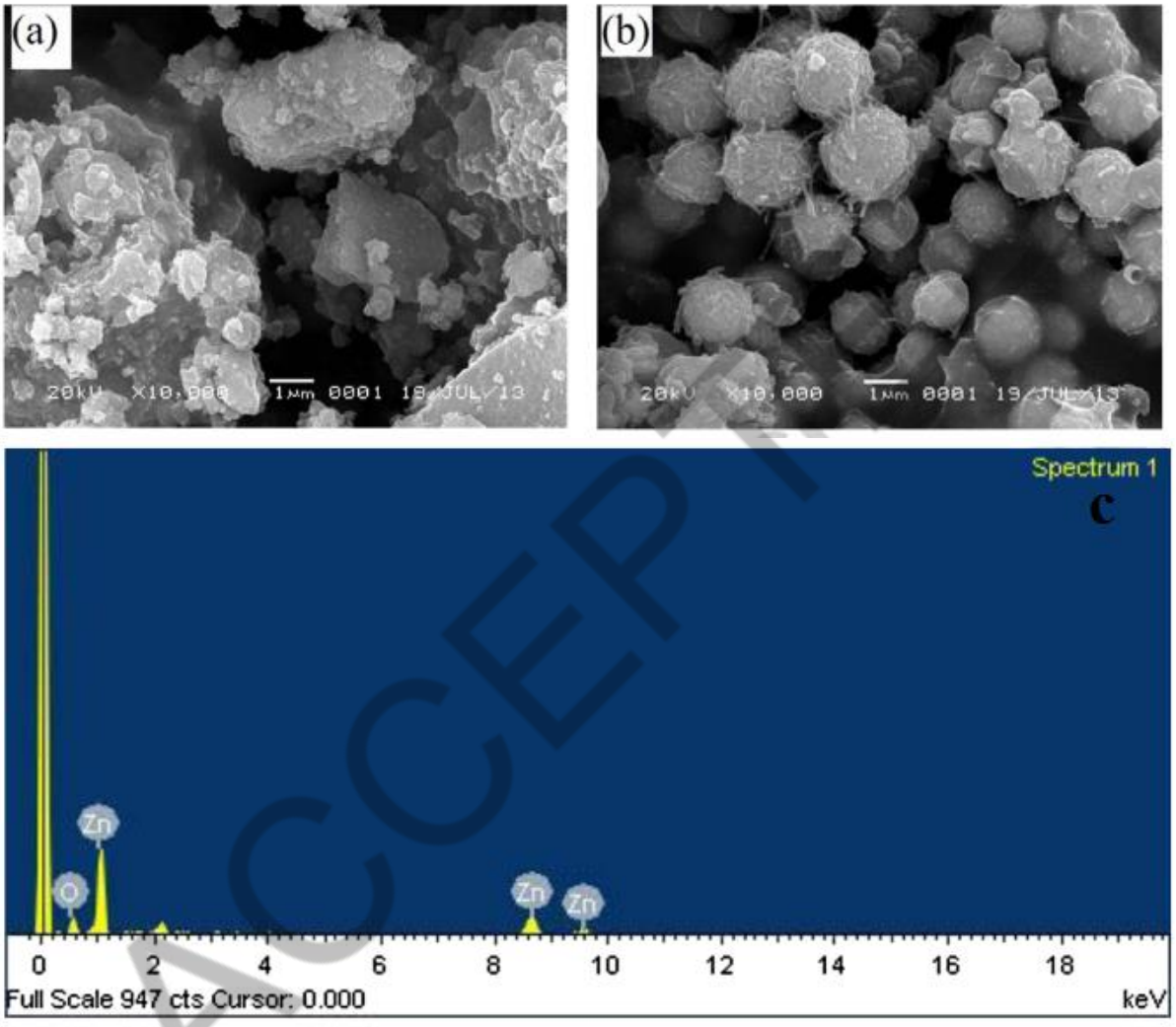


Figure 2. Images of a,b) FESEM and c) EDX spectrum of ZnO nanomaterials.

Figure 3 a and b illustrates the heat release rate and cylinder pressure, respectively, for test fuel blends at maximum load for a 7-hole fuel injector. At all, crank angles for TRCC and 7-hole FI due to better air and fuel mixing and high activation energy of ZnO nanoparticles that result in an enhanced swirl and squish movement within the piston bowl [22]. The viscosity and lower heating magnitude of the MOME20 lower the cylinder pressure. Hence, a maximum cylinder pressure of 51.9 bar was observed for MOME20 at 365 °CA. At maximum load, the cylinder pressure found for MOME2030 (MOME20+30 ppm ZnO) was 57.9 bar, the cylinder pressure improves due to the catalytic efect, shorter ignition delay, the higher surface area of ZnO nanoparticles [23-25].

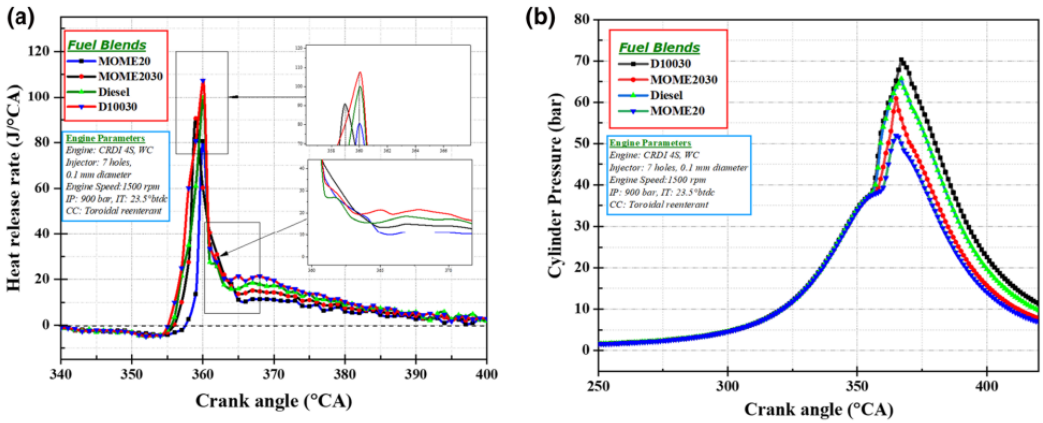


Figure 3. Variation of (a) heat release rate and (b) cylinder pressure at different crank angles.

This research has succeeded in making a fuel heating tank that was installed directly in the tank. The heater was a nickeline wire connected to an electric current. The result of heating the fuel is in the form of gas that was accommodated in a cylindrical gas tank which is also embedded in the fuel tank unit. The main components of the tank consist of; heating unit, thermoreader, fuel tank, gas tank, heat sink unit, tank cover, and wiring circuit. The data obtained is in the form of $O_2$, CO, HC, and $CO_2$ exhaust gas emissions, table 1. Table 2 shows the value of lamda and AFR test results using a gas analyzer.

Table 1. The results of the emission test ($O_2$, CO, $CO_2$, and HC).

| T (°C) | 3 bar (Pressure) | | | | | | | | | | | | 5 bar (Pressure) | | | | | | | | | | | |
|---|---|---|---|---|---|---|---|---|---|---|---|---|---|---|---|---|---|---|---|---|---|---|---|---|
| | 1000 rev/min | | | | 2000 rev/min | | | | 3000 rev/min | | | | 1000 rev/min | | | | 2000 rev/min | | | | 3000 rev/min | | | |
| | $O_2$ (%) | CO (%) | $CO_2$ (%) | HC (ppm) | $O_2$ (%) | CO (%) | $CO_2$ (%) | HC (ppm) | $O_2$ (%) | CO (%) | $CO_2$ (%) | HC (ppm) | $O_2$ (%) | CO (%) | $CO_2$ (%) | HC (ppm) | $O_2$ (%) | CO (%) | $CO_2$ (%) | HC (ppm) | $O_2$ (%) | CO (%) | $CO_2$ (%) | HC (ppm) |
| 25 | 12.5 | 2.40 | 5.00 | 2705 | 7.68 | 2.74 | 9.2 | 2537 | 8.65 | 3.1 | 7.9 | 2450 | 11.1 | 5.4 | 4.3 | 2804 | 7.79 | 4.34 | 8 | 2648 | 7.07 | 4.66 | 8.6 | 2445 |
| 50 | 11.4 | 3.70 | 5.90 | 2279 | 11.12 | 2.95 | 7.9 | 1966 | 8.78 | 2.5 | 8.5 | 2350 | 13.5 | 4.6 | 4.9 | 2606 | 12.3 | 4.1 | 8.2 | 2348 | 10.2 | 3.5 | 8.5 | 1559 |
| 75 | 11.6 | 3.50 | 5.20 | 2189 | 8.3 | 3.95 | 8.9 | 1726 | 9.98 | 2.9 | 8.2 | 2421 | 12.5 | 4.5 | 4.5 | 2707 | 8.32 | 4 | 7 | 2558 | 10.3 | 3.27 | 8.5 | 2549 |
| 100 | 15.50 | 3.28 | 5.50 | 1987 | 11.75 | 2.77 | 7.9 | 1899 | 14.8 | 1.97 | 9.2 | 1910 | 15.8 | 3.9 | 5.3 | 2522 | 12.4 | 3.24 | 8.5 | 1987 | 15.8 | 2.87 | 9.3 | 2365 |

Table 2. The results of the Lambda and AFR emission test.

| T (°C) | 3 bar (Pressure) | | | | | | 5 bar (Pressure) | | | | | |
|---|---|---|---|---|---|---|---|---|---|---|---|---|
| | 1000 rev/min | | 2000 rev/min | | 3000 rev/min | | 1000 rev/min | | 2000 rev/min | | 3000 rev/min | |
| | Lambda | AFR | Lambda | AFR | Lambda | AFR | Lambda | AFR | Lambda | AFR | Lambda | AFR |
| 25 | 1.702 | 25.00 | 1.157 | 17.00 | 1.228 | 18.00 | 1.309 | 19.20 | 1.124 | 16.50 | 1.066 | 15.60 |
| 50 | 1.630 | 13.90 | 1.275 | 15.80 | 1.425 | 16.90 | 1.650 | 17.20 | 1.532 | 16.90 | 1.450 | 17.20 |
| 75 | 1.720 | 14.90 | 1.150 | 16.80 | 1.122 | 17.90 | 1.734 | 19.20 | 1.424 | 16.50 | 1.734 | 15.60 |
| 100 | 1.927 | 12.40 | 1.845 | 14.50 | 1.656 | 16.40 | 1.987 | 15.20 | 1.766 | 16.40 | 1.987 | 18.20 |

Figure 4a shows that the oxygen produced from the Pertamax fuel with a fuel pressure of 3 bar is the highest at 15.50 % at 100 °C at 1000 rpm. This shows that this test is rich in oxygen ($O_2$). Based on Figure 4b. shows that the oxygen content produced from Pertamax fuel with a fuel pressure of 5 bar is the highest at 100 °C with a rotation of 3000 rpm of 15.80 %, this shows that this test is rich in oxygen ($O_2$).

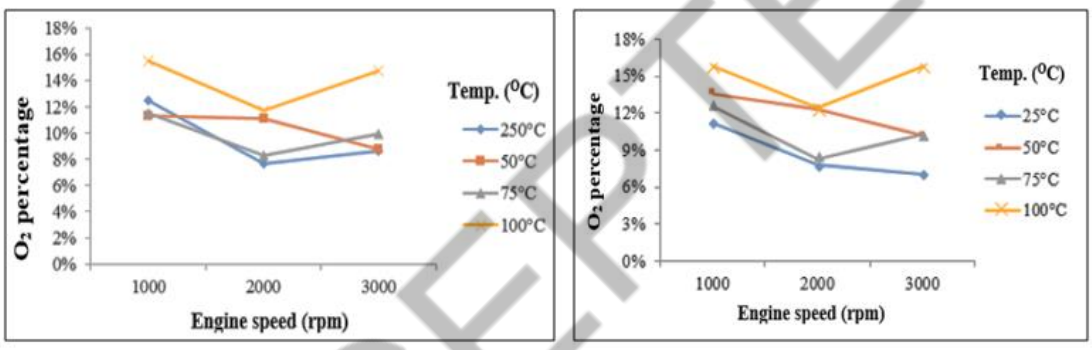


a. Pressure 3 bar b. Pressure 5 bar

Figure 4. $O_2$ emission amounts for the ZnO based fuel system at different temperatures.

According to research by AA Wira Kresna Ningrat [26], the $O_2$ exhaust emission content in Pertamax fuel has the lowest value of 11.99 % at 5000 rpm rotation. Figure 5a. show a fuel pressure of 3 bar with a temperature of 75 °C, the highest carbon monoxide value is 3.95 and the lowest value is 1.97 at 100 °C at 3000 rpm. It can be concluded that at a pressure of 3 bar of fuel, Pertamax, the best CO level is at a temperature of 100 °C at 3000 rpm. CO was related to the mixture of fuel and air, the smaller the CO level, the more economical and vice versa. According to figure 4b, it can be concluded that at a fuel pressure of 5 bar with a temperature of 25 °C, the highest carbon monoxide value is 5.43 and the lowest value is in the number 2.87 at 100°C and 3000 rpm rotation. At temperatures of 50 and 75 °C, there is no significant difference, it's just that it looks different at 3000 rpm. A temperature of 100 degrees Celsius has the lowest CO level with a decrease of 25.45 %.

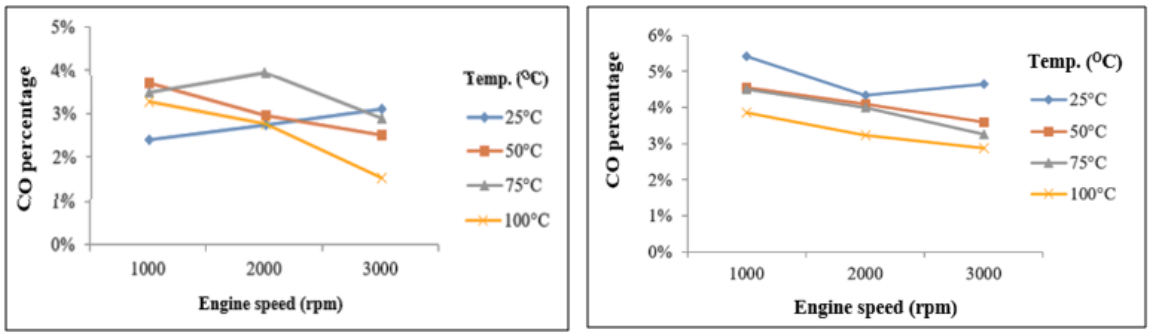


a. Pressure 3 bar b. Pressure 5 bar

Figure 5. CO emission amounts for the ZnO based fuel system at different temperatures.

Figure 6a shows the levels of carbon dioxide ($CO_2$) emissions from the research results. The highest carbon dioxide level is at 100 °C at 3000 rpm with several 9.2, while the lowest value is at 25 °C with a 1000 rpm rotation of 5.0 %. Figure 6b shows the level of carbon dioxide ($CO_2$) from the exhaust emission test results at a pressure of 5 bar. The highest carbon dioxide level is at 100 °C at 3000 rpm, while the lowest value is at 25 °C with 1000 rpm rotation. So that in general the $CO_2$ emission for this study is still very good, with the highest $CO_2$ level being 9.3 %.

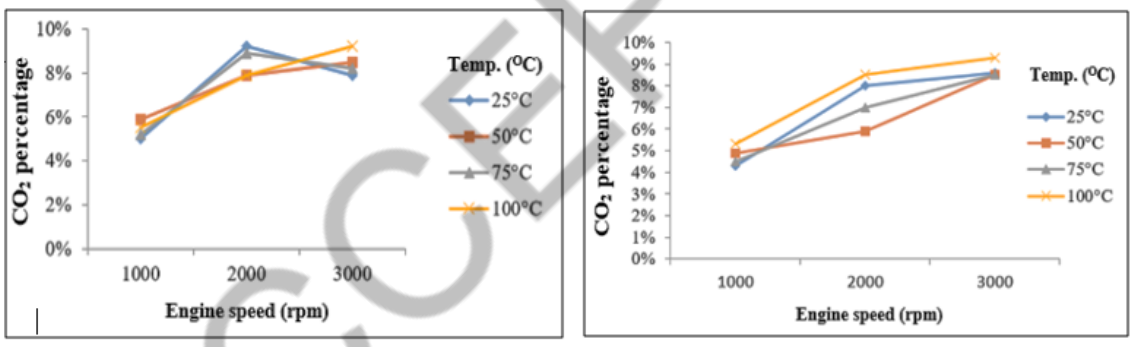


a. Pressure 3 bar b. Pressure 5 bar

Figure 6. $CO_2$ emission amounts for the ZnO based fuel system at different temperatures.

Figure 7a shows the level of Hydrocarbon (HC) at 3 bar fuel pressure using Pertamax fuel. The highest HC level is at 25 °C at 1000 rpm with 2705 ppm, while the lowest HC level is at 100 °C at 3000 rpm with 1910 ppm. HC emission levels indicate combustion under over-fuel conditions or fuel shortages. Figure 7b. shows the level of Hydrocarbon (HC) at 5 bar fuel pressure using Pertamax fuel. The highest HC level is at a temperature of 25 °C degrees at 1000 rpm with a figure of 2606 ppm, while the lowest HC level is at a temperature of 100 °C degrees at 2000 rev/min with a figure of 1987 ppm. The HC level indicates the presence of unburned fuel [27]. The lowest decrease in HC levels occurred at a temperature of 100 degrees Celsius with a rotation of 3000 rpm which was

6.23 %. The HC level decreases if the engine speed is higher, this indicates that a heated tank system can increase combustion [28].

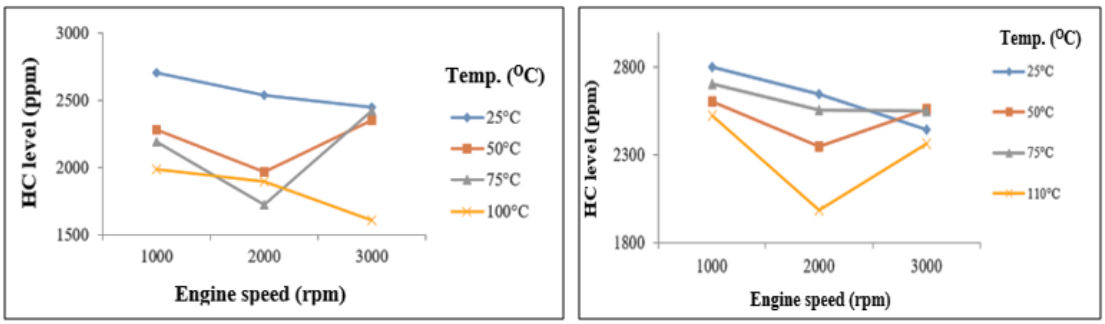


a. Pressure 3 bar b. Pressure 5 bar

Figure 7. HC emission amounts for the ZnO based fuel system at different temperatures

Figure 8a shows the lambda value of exhaust emission testing on the engine using a nano fuel system tank. The highest lambda value lies at a temperature of 100 °C with a rotation of 1000 rpm which indicates that temperatures of 100 °C and 1000 rpm have good air in the engine (rich in the air). The lowest lambda result is at a temperature of 25 °C at 2000 rpm with the number 1157 ppm. Figure 8b shows the results of the lambda value from testing exhaust emissions on the engine using a nano fuel system tank. The highest lambda value lies at a temperature of 100 °C with a rotation of 1000 rpm which indicates that temperatures of 100 degrees and 1000 rpm have good air in the engine (rich in the air). The lowest lambda yield was located at a temperature of 25 °C with a rotation of 3000 rev/min at 1066 ppm.

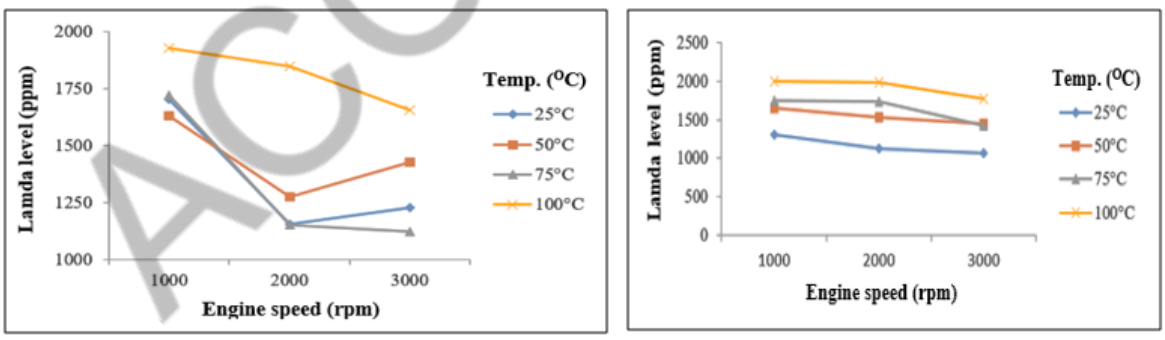


a. Pressure 3 bar b. Pressure 5 bar

Figure 8. Lambda levels for the ZnO based fuel system at different temperatures.

Figure 9a shows the air-fuel ratio produced from the engine using a nano fuel system tank. Air Fuel Ratio content affects the power of the engine itself, if the air-fuel ratio is thin then fuel consumption becomes efficient and engine power is slightly reduced. The highest AFR levels are at 25 °C with 1000 rpm and the lowest AFR levels are located at 100 °C at 1000 rpm at 12.4. Figure 9b shows the air-fuel ratio produced from the engine using a nano fuel system tank. The highest AFR level is at 100 °C with 2000 rpm and the lowest AFR is at 100 °C at 1000

rpm at 11.4. In general, AFR levels indicate a fuel-rich value. This indicates that fuel in the form of gas is easier to supply, where the trend of spin rises then AFR levels rise.

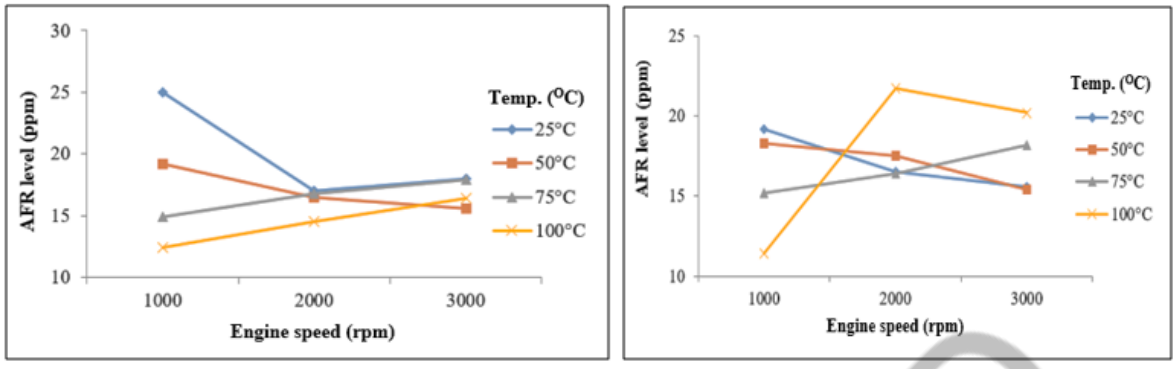


a. Pressure 3 bar b. Pressure 5 bar

Figure 9. Air Fuel Ratio (AFR) levels for the ZnO based fuel system at different temperatures.

## 4. Conclusion

CO levels decreased as the average fuel temperature rose by 7 % at 3 bar pressure and 25.45 % at 5 bar pressures. This indicates that the presence of a heated fuel tank will lower the level of exhaust emissions. The heated fuel tank installed resulted in better combustion, both seen in the lowest HC levels at 1000 °C with a 3000-rpm rotation of 6.23 %. So, the installation of a heated fuel tank will decrease fuel consumption. The resulting carbon dioxide emission levels indicate that they are below the standard $CO_2$ emission limit. Besides, it was found that increasing aqueous N-Alumina volume fraction reduced exhaust gas temperatures. The reductions were 2.9%, 14.4%, 14.63, 20% and 30% for 1%, 3%, 5%, 7% and 10% of N-$Al_2O_3$ emulsion blends respectively compared to diesel.


## Acknowledgments

We would like to thank LPPM Sekolah Tinggi Teknologi "Warga" Surakarta, Lecturers and Heavy equipment laboratory, and student research team.


## References


[1] A. V. Porsin, S. G. Tsarichenko, Y. A. Dobrovol'skii, A. V. Kozlov, G. G. Nadareishvili, and A. S. Terenchenko, "Analysis of the Safety of Using Hydrocarbon Fuels and Hydrogen in Automobiles," Russ. J. Appl. Chem., vol. 93, no. 10, pp. 1604–1614, 2020, doi: 10.1134/S10704272201016X.

[2] L. Proskuryakova, "Foresight for the 'energy' priority of the Russian Science and Technology Strategy," Energy Strateg. Rev., vol. 26, no. July 2018, p. 100378, 2019, doi: 10.1016/j.esr.2019.100378.

[3] Z. Abdin, A. Zafaranloo, A. Rafiee, W. Mérida, W. Lipiński, and K. R. Khalilpour, “Hydrogen as an energy vector,” Renew. Sustain. Energy Rev., vol. 120, no. May 2019, 2020, doi: 10.1016/j.rser.2019.109620.

[4] W. W. Pulkrabek, “Engineering Fundamentals of the Internal Combustion Engine,” J. Chem. Inf. Model., vol. 53, no. 9, pp. 1689–1699, 2013.

[5] J. D. Halderman, Halderman J.D. Automotive Technology_ Principles, Diagnosis, and Service (Part 1) - libgen.lc.pdf. 2012.

[6] R. Safira, W. Ruslan, and O. T. Swan, “Experimental Case Study on the Impact of the Implementation of Hydrocarbon Crack System with Bioethanol or RON 92 Gasoline as an Addition on the Performance of a Toyota Corolla Twincam AE92,” Int. J. Apllied Eng. Res., vol. 13, no. 2, pp. 1442–1449, 2018.

[7] D. Rohmantoro, B. G. Purnomo, M. Amiruddin, and S. Mahendra, “Analysis of the Effect of A Catalyst Hydrocarbon Crack System Spiral Pipe against the 4-Stroke Motorcycle Engine Power,” J. Phys. Conf. Ser., vol. 1823, no. 1, 2021, doi: 10.1088/1742-6596/1823/1/012047.

[8] E. Suryono, I. H. A. Nagoro, and D. Y. S. Wicaksana, “Analisis Temperatur Bahan Bakar pada Reaktor Hydrocarbon Crack System Terhadap Hasil Emisi Engine 4A-FE,” Automot. Exp., vol. 1, no. 03, pp. 58–63, 2018, doi: 10.31603/ae.v1i03.2333.

[9] D. Olsson, “Comparisson of reforming process between different types of biogas reforming reactors,” 2008.

[10] V. Markov, V. Kamaltdinov, S. Devyanin, B. Sa, A. Zherdev, and V. Furman, “Investigation of the Influence of Different Vegetable Oils as a Component of Blended Biofuel on Performance and Emission Characteristics of a Diesel Engine for Agricultural Machinery and Commercial Vehicles,” Resources, vol. 10, no. 74, pp. 22–23, 2021.

[11] H. Hazar and H. Sevinc, “Investigation of the effects of pre-heated linseed oil on performance and exhaust emission at a coated diesel engine,” Renew. Energy, vol. 130, pp. 961–967, 2019, doi: 10.1016/j.renene.2018.07.003.

[12] N. L. Jain, S. L. Soni, M. P. Poonia, D. Sharma, A. K. Srivastava, and H. Jain, “Performance and emission characteristics of preheated and blended thumba vegetable oil in a compression ignition engine,” Appl. Therm. Eng., vol. 113, pp. 970–979, 2017, doi: 10.1016/j.applthermaleng.2016.10.186.

[13] A. Budiprasojo and A. Irawan, “Engine Combustion Efficiency and Performance of Exhaust Pipe Fuel Preheating System,” J. Rekayasa Mesin, vol. 9, no. 1, pp. 1–7, 2018, doi: 10.21776/ub.jrm.2018.009.01.1.

[14] P. Kolbitsch, C. Pfeifer, and H. Hofbauer, “Catalytic steam reforming of model biogas,” Fuel, vol. 87, no. 6, pp. 701–706, 2008, doi: 10.1016/j.fuel.2007.06.002.

[15] Yang, Z. & Liu, Q.-H. Te structural and optical properties of ZnO nanorods via citric acid-assisted annealing route. J. Mater. Sci. 43, 6527–6530 (2008).

[16] Znaidi, L., Illia, G. S., Benyahia, S., Sanchez, C. & Kanaev, A. Oriented ZnO thin flms synthesis by sol–gel process for laser application. Tin Solid Films 428, 257–262 (2003).

[17] Johnson, M., Powell, D. & Cannon, R. Vibrational spectra of carboxylato complexes—II. Some oxo-tetranuclear complexes. Spectrochim. Acta Part A Mol. Spectrosc. 38, 125–131 (1982).

[18] Dhinesh, B., Annamalai, M., Lalvani, I. J. & Annamalai, K. Studies on the infuence of combustion bowl modifcation for the operation of Cymbopogon fexuosus biofuel based diesel blends in a DI diesel engine. Appl. Term. Eng. 112, 627–637 (2017).

[19] Karthikeyan, S., Elango, A. & Prathima, A. Performance and emission study on zinc oxide nano particles addition with pomolion stearin wax biodiesel of CI engine. JSIR. 73, 187–190 (2014).

[20] Karthikeyan, S., Elango, A. & Prathima, A. An environmental efect of GSO methyl ester with ZnO additive fuelled marine engine. IJMS. 43, 564–570 (2014).

[21] Karthikeyan, S., Elango, A. & Prathima, A. Diesel engine performance and emission analysis using canola oil methyl ester with the nano sized zinc oxide particles. IJEMS. 21, 83–87 (2014).

[22] A. A. W. K. Ningrat, I. G. B. W. Kusuma, and I. Wayan, "Pengaruh Penggunaan Bahan Bakar Pertalite Terhadap Akselerasi," Mettek, vol. 2, no. 1, pp. 59–67, 2016.

[23] S. Raharjo and Solechan, "Studi pengaruh penambahan pipa katalis," in Simposium Nasional Teknologi Terapan (SNTT), 2013, pp. 28–34.

[24] Mastur, K. Setiawan, and T. D. Susanto, "Desain Kritis Pipa Katalis Berbahan Copper Dan Aluminium Pada Hydrocarbon Crack System (HCS) Untuk Optimasi Pembakaran Motor Bensin dan Penurun Emisi Gas Buang," Pros. Semin. Nas. Unimus, vol. 1, pp. 688–696, 2018.

[25] K. Jayaraman, K.V. Anand, S.R. Chakravarthy, R. Sarathi, Effect of nano-aluminum in plateau-burning and catalyzed composite solid propellant combustion, Combust. Flame 156 (2010) 1662–1673.

[26] J.L. Sabourin, R.A. Yetter, B.W. Asay, J.M. Lloyd, V.E. Sanders, G.A. Risha, S.F. Son, Effect of nano-aluminum and fumed silica particles on deflagration and detonation of nitro-methane, Propellants Explos. Pyrotech. 34 (2009) 385–393.

[27] C.H. Li, G.P. Peterson, Experimental investigation of temperature and volume fraction variations on the effective thermal conductivity of nano-particle suspensions (nano-fluids), J. Appl. Phys. 99 (2006) 084314.

[28] ASHREA Giude Line, Guide Engineering Analysis of Experimental Data, Guideline 2, 1986.